Precision Position/Force Interaction Control of a Piezoelectric Multimorph Microgripper for Microassembly

Qingsong Xu, *Member, IEEE*

***Abstract*—Precision position and force control is a critical issue for automated microassembly systems to handle micro-objects delicately. This paper presents two new approaches to regulating both position and contact force of a piezoelectric multimorph microgripper dedicated to microassembly tasks. One of the advantages of the proposed approaches lies in that they are capable of controlling the position and contact force of a gripper arm simultaneously. The methodology is easy to implement since neither a state observer nor a hysteresis model of the system is required. The first approach is a position-based sliding mode impedance control which converts the target impedance into a desired position trajectory to be tracked, and the second one is established on the basis of a proportional-integral type of sliding function of the impedance measure error. Their tracking performances are guaranteed by two devised discrete-time sliding mode control algorithms, whose stabilities in the presence of model uncertainties and disturbances are proved in theory. The effectiveness of both schemes are validated by experimental investigations on a glass microbead gripping task. Results show that both approaches are capable of accomplishing promising interaction control accuracy.**

***Note to Practitioners*—In view of the requirements of simultaneous position and force regulations for gripping operation in microassembly, two new interaction control schemes are presented in this paper. Specifically, microgrippers which are composed of two piezoelectric cantilever actuators are investigated. Conventionally, the position is controlled for one gripper arm and the force is controlled for the other one. Hence, two controllers require to be designed and both arms need to be actuated, which complicates the control design process and imposes higher hardware cost. By employing the proposed control schemes, one single controller is sufficient to control both position and force of a single arm of the microgripper. This indicates a significant reduction on both control design workload and hardware cost. To implement the reported control strategies, only a second-order dynamics model of the system is required. Hence, these digital controllers can be easily deployed to sampled-data microassembly systems. Through the gripping test of a microbead, experimental studies demonstrate that a precise position and force tracking control is achieved simultaneously by the proposed approaches.**

***Index Terms*—Force control, impedance control, microassembly, micromanipulation, piezoelectric actuator, position control.**

Manuscript received August 19, 2012; revised November 26, 2012; accepted December 20, 2012. Date of publication January 28, 2013; date of current version June 27, 2013. This paper was recommended for publication by Associate Editor C. Clevy and Editor K. Bohringer upon evaluation of the reviewers' comments. This work was supported in part by the Macao Science and Technology Development Fund under Grant 024/2011/A and in part by the Research Committee of the University of Macau under Grant MYRG083(Y1-L2)-FST12-XQS.

The author is with the Department of Electromechanical Engineering, Faculty of Science and Technology, University of Macau, Macao, China (e-mail: qsxu@umac.mo).

Color versions of one or more of the figures in this paper are available online at http://ieeexplore.ieee.org.

Digital Object Identifier 10.1109/TASE.2013.2239288

I. Introduction

In either industrial assembly lines or biomedical research laboratories, the manipulation and assembly of objects in micro- and nanometer scales pose great challenges to even skilled human operators. Hence, automated robotic microassembly systems are necessary to cater for the accuracy and efficiency requirements [1]–[3]. Microgripper is one of the crucial devices in the aforementioned applications. Various types of microgrippers have been proposed in the literature, such as electrostatic [4], electrothermal [5], and piezoelectric microgrippers [6], according to different actuation principles. Particularly, as a typical smart actuator, piezoelectric actuator is attractive owing to its merits of subnanometer positioning resolution and rapid response speed. Hence, piezoelectric microgrippers which are composed of two piezoelectric unimorph, bimorph, or multimroph actuators are popularly applied in micromanipulation and microassembly.

However, the piezoelectric nonlinearities in terms of hysteresis and creep effects impose an obstacle to precise positioning control of piezoelectric microgrippers [7]. According to the driving principle, both charge (or current) drives and voltage drives have been employed. The former are capable of alleviating the hysteresis effect significantly [8]–[10]. However, it is at the sacrifice of a reduced stroke. Hence, the latter voltage drives are still widely adopted in practice. Generally, the existing voltage drives fall into two categories in terms of hysteresis model-based and hysteresis model-free approaches. Although the hysteresis effect can be well compensated for by constructing a feedforward control based on an inverse hysteresis model in the first approach [7], [11], it is a time-consuming work and the positioning accuracy is very sensitive to the accuracy of the established model [12]. Moreover, the creep (or drift) phenomenon needs an extra treatment [13]. Thus, the second approach, which relies on the design of a feedback control [14]–[16], is more attractive from practical implementation point-of-view. In particular, sliding mode control (SMC) has demonstrated its potential in precise motion control in the presence of model uncertainties and external disturbances [17]. Hence, SMC strategy has been widely adopted in positioning control of piezoelectric actuated systems [18], [19].

Nonetheless, to handle micro-objects delicately while without damaging the microgripper and objects, an appropriate adjustment of the contact force between the gripper arms and objects is indispensable. Therefore, the control of both position and contact force is required in a microassembly system for regulating the interaction between the gripper arms and objects [20]. Unfortunately, as compared with the numerous works on position control, the research dedicated to interaction control

of piezoelectric microgrippers is rare to find [21]. Indeed, the requirement of simultaneous control of both position and contact force for a gripper arm poses a great challenge in microgripping tasks. In majority of previous works, one gripper arm has been controlled with respect to either position or force alone [5], [22], which is not sufficient to accomplish a safe microassembly task. Recently, the control of both position and force has been successfully realized in [21]. This control strategy was implemented on a hybrid thermo-piezoelectric microgripper by performing position control of the right arm and force control of the left arm, respectively. Thus, it requires the design of two controllers and the actuation of both arms, which complicates the control design process and imposes higher cost on the hardware. Practically, the simultaneous position and force control of one gripper arm is desirable from the viewpoint of reliable interaction as well as workload and hardware cost reduction.

In the macroscale, there are generally two basic approaches to interaction control, namely, hybrid position/force control and impedance control. The former method decomposes the task space of the end-effector into orthogonal position subspace and force subspace by resorting to the selection matrix. However, a switching of control law is required to implement the position control in position subspace and force control in force subspace alternately [23], [24]. Alternatively, instead of controlling the position or contact force of the end-effector, the objective of the latter impedance control is to regulate a desired dynamic relation between the position and contact force along the same direction [25]–[27]. In this way, both position and force are controlled simultaneously by regulating the predefined dynamic response, i.e., the target impedance. Hence, different from the hybrid position/force control, the impedance control can be used to regulate the position and force at the same time. For instance, the simultaneous position and force control of some one-degree-of-freedom (1-DOF) systems have been reported in the literature [28], [29]. Therefore, the impedance control emerges as a promising strategy for a delicate interaction control in microscale [29]–[31].

Combining with the aforementioned SMC technique, the concept of sliding-mode impedance control has been reported in previous works [23], [32]. However, it was implemented in continuous-time form. In practice, the control scheme of a microassembly system is usually realized by resorting to a computer or a digital-signal-processing (DSP) apparatus, i.e., a sampled-data system. Deploying a continuous-time controller directly to a digital system may cause severe instability of the system, especially when the sampling frequency is not high. Thus, to realize a stable controller on a sampled-data system, a discrete-time impedance control is more desirable [33]. Although the pseudo-continuous time control method also works for sampled-data systems [34], it is mainly intended for linear time-invariant systems. Hence, the direct discrete-time control is more suitable for nonlinear piezoactauted systems. Nevertheless, to the knowledge of the author, no discrete-time sliding mode impedance control scheme has been reported in the literature.

The objective of this paper is to develop an interaction control framework for a piezoelectric microgripper in order to control the position and contact force simultaneously. Specifically, two new control schemes of discrete-time impedance control in conjunction with discrete-time sliding mode control (DSMC) are proposed for an interaction control of a sampled-data microassembly system. Instead of modeling the complicated piezoelectric (hysteresis and creep) effects as conducted in existing works, the unmodeled nonlinearities and other uncertainties/disturbances are treated as a lumped perturbation, which simplifies the control design procedure. By making use of the generalized impedance control methodology [35], the position and interaction force are regulated simultaneously and smoothly. Instead of driving two arms, the actuation of a single gripper arm is sufficient for microassembly tasks using the proposed interaction control schemes.

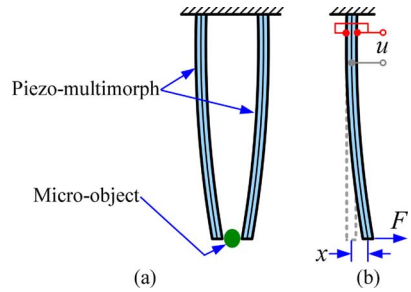

Fig. 1. (a) Illustration of a micro-object gripping by a piezoelectric microgripper which is composed of two piezoelectric multimorphs. (b) Output displacement x of a piezoelectric multimorph cantilever under the excitation of input voltage u and external force F.

The rest of this paper is organized as follows. Based on the dynamics model of a piezoelectric cantilever arm, the interaction control problem is formulated in Section II. Then, a position-based sliding mode impedance control (PBSMIC) scheme and a discrete-time sliding mode impedance force control (DSMIFC) scheme are developed in Sections III and IV, respectively. Stability analyses of the control systems are performed in detail. A theoretical comparison and analysis of the two control schemes is presented in Section V. Afterwards, experimental studies on a microbead gripping are carried out in Section VI to verify the effectiveness of the devised schemes. Discussions cover tracking performances, force estimator development, concurrent trajectory planning, and dynamics and controller parameters setting. Finally, conclusion is briefly exposed in Section VII.

II. Dynamics Modeling and Problem Formulation

Fig. 1(a) illustrates a microgripper constructed by two piezoelectric multimorphs for manipulating a micro-object. Due to the symmetry of the gripper, one gripper arm, i.e., a piezoelectric cantilever as shown in Fig. 1(b) is picked out for a detailed analysis. It is observed that the cantilever suffers from an excitation voltage u and a contact force F which is applied by the micro-object. The overall output displacement is described by x. In order to guarantee a safe interaction between the gripper and micro-object during the manipulation, both the position and contact force need to be well controlled.

A. Dynamics Modeling and Perturbation Estimation

Dynamics model provides a base for the control system design. The modeling of piezoactuated systems has been investigated in a great number of previous works. Although the linear

part of the system can be described by a higher order model, a second-order one is employed due to its popularity [36], [37].

The dynamics model of a piezoelectric cantilever under both actions of input voltage and external force can be established as follows [36]:

$$m\ddot{x}(t) + b\dot{x}(t) + kx(t) = du(t) + p(t) - F(t) \tag{1}$$

where t is the time variable, parameters m, b, k, and x represent the mass, damping coefficient, stiffness, and output displacement of the gripper arm, respectively; d is the piezoelectric coefficient, u denotes the input voltage, F is the interaction force, and the lumped perturbation term p describes the combined effects of piezoelectric nonlinearity (in terms of hysteresis and creep effects) as well as other model uncertainties and disturbances.

By adopting a small sampling time T, the following approximations are valid [33], [38]:

$$\dot{x}(t) \approx \frac{1}{T}[x(kT) - x(kT - T)] \tag{2}$$

$$\ddot{x}(t) \approx \frac{1}{T^2}[x(kT) - 2x(kT - T) + x(kT - 2T)] \tag{3}$$

where k denotes the kth time step.

Then, the continuous-time dynamics model (1) can be converted into an equivalent discrete-time form

$$\bar{m}x_{k-2} + \bar{b}x_{k-1} + \bar{k}x_k = \bar{d}u_k + p_k - F_k \tag{4}$$

where $x_k = x(kT)$ and

$$\bar{m} = \frac{m}{T^2},\ \bar{b} = -\frac{2m}{T^2} - \frac{b}{T},\ \bar{k} = \frac{m}{T^2} + \frac{b}{T} + k,\ \bar{d} = d. \tag{5}$$

Traditionally, the hysteresis and creep effects are analytically modeled based on various types of models [7], [11], [36]. Nevertheless, the modeling procedure is time-consuming and model errors always exist. In this paper, the lumped perturbation term p_k is derived by its one-step delayed estimation by employing the perturbation estimation technique [37], [39]

$$\hat{p}_k = p_{k-1} = -\bar{d}u_{k-1} + \bar{m}x_{k-3} + \bar{b}x_{k-2} + \bar{k}x_{k-1} + F_{k-1}. \tag{6}$$

Thus, the dynamics model (4) can be rewritten into

$$\bar{m}x_{k-2} + \bar{b}x_{k-1} + \bar{k}x_k = \bar{d}u_k + \hat{p}_k - \tilde{p}_k - F_k \tag{7}$$

where $\tilde{p}_k = \hat{p}_k - p_k$ is the perturbation estimation error, which can be further expressed as follows:

$$\tilde{p}_k = p_{k-1} - p_k \approx -\dot{p}(t)\,T. \tag{8}$$

In this research, it is assumed that the first derivative of the perturbation term is bounded, i.e., $|\dot{p}(t)| \le \Delta$. Then, it can be deduced that

$$|\tilde{p}_k| \le \Delta T \tag{9}$$

which indicates that the perturbation estimation error is also bounded.

B. Impedance Control Framework

In view of the limitation of conventional impedance control [40], the generalized impedance control (GIC) scheme has been developed [35] to relate the position error to the interaction force error by a generalized impedance equation

$$M(\ddot{x} - \ddot{x}_r) + B(\dot{x} - \dot{x}_r) + K(x - x_r) = -K_f(F - F_r) \tag{10}$$

where M, B, K, and K_f are desired parameters for the generalized impedance. Besides, x_r and x represent the predefined reference and actual gripper output position, F_r and F denote the desired and actual contact force, respectively. By introducing the reference force F_r, the interaction force can be explicitly controlled by GIC approach, which is the improvement as compared with conventional impedance control.

By assigning a position error

$$\tilde{e} = x - x_r \tag{11}$$

the differential (10) can be equivalently converted into the difference equation

$$\bar{M}\tilde{e}_{k-2} + \bar{B}\tilde{e}_{k-1} + \bar{K}\tilde{e}_k = -\bar{K}_f(F_k - F_{r,k}) \tag{12}$$

where $\tilde{e}_k = \tilde{e}(kT)$ with T denoting the sampling time.

Taking into account the approximations (2) and (3), the relationships between the target parameters of continuous-time (M, B, K, and K_f) and discrete-time ($\bar{M}$, $\bar{B}$, $\bar{K}$, and $\bar{K}_f$) models are derived below

$$\bar{M} = \frac{M}{T^2},\ \bar{B} = -\frac{2M}{T^2} - \frac{B}{T},\ \bar{K} = \frac{M}{T^2} + \frac{B}{T} + K,\ \bar{K}_f = K_f. \tag{13}$$

In order to guarantee the achievement of the desired impedance behavior (12) in the presence of uncertainties and disturbances, two discrete-time sliding mode-based robust control schemes are proposed in the subsequent sections.

III. PBSMIC Scheme Design

By solving the desired position trajectory from the target impedance relationship, a position-based impedance control is presented in this section.

Once the four target impedance parameters (M, B, K, and K_f) of the generalized impedance (10) are defined according to pertinent applications, the control objective can be realized if the gripper position x closely tracks the desired position trajectory x_d, which is defined by the following impedance filter:

$$M\ddot{x}_d + B\dot{x}_d + Kx_d = -K_f(F - F_r) + M\ddot{x}_r + B\dot{x}_r + Kx_r \tag{14}$$

with initial conditions

$$x_d(0) = x_r(0), \quad \dot{x}_d(0) = \dot{x}_r(0). \tag{15}$$

It is observed from (14) that $x_d = x_r$ holds in free space without the contact force F if the desired force is $F_r = 0$. Otherwise, in the presence of F, the desired trajectory x_d needs to be solved from (14).

In view of (12), the solution of the desired trajectory in the discrete-time form can be obtained from (14):

$$\begin{aligned} x_{d,k} = {} & -\bar{K}^{-1}\bar{M}(x_{d,k-2} - x_{r,k-2}) \\ & -\bar{K}^{-1}\bar{B}(x_{d,k-1} - x_{r,k-1}) - \bar{K}^{-1}\bar{K}_f(F_k - F_{r,k}) + x_{r,k} \end{aligned} \tag{16}$$

where the parameters $\bar{M}$, $\bar{B}$, $\bar{K}$, and $\bar{K}_f$ are given in (13).

Thus, with the impedance parameters ($\bar{M}$, $\bar{B}$, $\bar{K}$, and $\bar{K}_f$), the impedance control is converted into the position tracking control of the trajectory (16). In the subsequent discussions, a DSMC strategy is developed to realize the position-based impedance control.

A. DSMC Design

First, substituting (6) into (7) allows the calculation of the position value

$$x_k = \frac{1}{\bar{k}}[\bar{d}(u_k - u_{k-1}) + \bar{m}x_{k-3} + (\bar{b} - \bar{m})x_{k-2} + (\bar{k} - \bar{b})x_{k-1} - (F_k - F_{k-1}) - \tilde{p}_k]. \quad (17)$$

Based on the position error $e_k = x_k - x_{d,k}$, a proportional-integral (PI)-type sliding function is defined as follows:

$$s_k = K_P e_k + K_I \varepsilon_k \quad (18)$$

where K_P and K_I are the proportional and integral gains, respectively. In addition, the integral error item is defined as

$$\varepsilon_k = \sum_{i=1}^{k} e_i = e_k + \varepsilon_{k-1}. \quad (19)$$

Considering that the equivalent control u_k^{eq} is the solution to $\Delta s_k = s_k - s_{k-1} = 0$ [41], the following deduction can be derived:

$$K_P e_k + K_I \varepsilon_k = s_{k-1} \quad (20)$$

$$\Rightarrow (K_P + K_I)e_k + K_I \varepsilon_{k-1} = s_{k-1} \quad (21)$$

$$\Rightarrow (K_P + K_I)(x_k - x_{d,k}) + K_I \varepsilon_{k-1} = s_{k-1}. \quad (22)$$

Then, inserting (17) into (22) and ignoring the estimation error $\tilde{p}_k$ leads to the equivalent control

$$u_k^{eq} = u_{k-1} + \frac{1}{\bar{d}}\left(\frac{\bar{k}}{G_a}s_{k-1} - \frac{\bar{k}}{G_a}K_I\varepsilon_{k-1} + \bar{k}x_{d,k}\right) - \frac{1}{\bar{d}}\left[\bar{m}x_{k-3} + (\bar{b} - \bar{m})x_{k-2} + (\bar{k} - \bar{b})x_{k-1} - (F_k - F_{k-1})\right] \quad (23)$$

where $G_a = K_P + K_I$.

The equivalent controller (23) takes effect in the sliding phase when the position trajectory is kept on the sliding surface (i.e., $s_k = 0$). However, if the initial position of the system does not lie on the sliding surface or large estimation error $\tilde{p}_k$ emerges due to large uncertainties and disturbances during the sliding phase, the standalone equivalent control cannot drive the position trajectory towards the sliding surface. Under such situations, an extra control action u_k^{sw} is necessary.

Thus, the equivalent control is augmented by a discontinuous control to give the total control action

$$u_k = u_k^{eq} + u_k^{sw} \quad (24)$$

i.e.,

$$u_k = u_{k-1} + \frac{1}{\bar{d}}\left(\frac{\bar{k}}{G_a}s_{k-1} - \frac{\bar{k}}{G_a}K_I\varepsilon_{k-1} + \bar{k}x_{d,k}\right) - \frac{1}{\bar{d}}\left[\bar{m}x_{k-3} + (\bar{b} - \bar{m})x_{k-2} + (\bar{k} - \bar{b})x_{k-1} - (F_k - F_{k-1})\right] - \frac{K_S}{\bar{d}}\mathrm{sgn}(s_{k-1}) \quad (25)$$

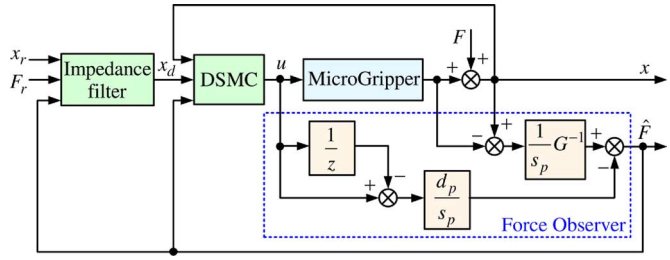

Fig. 2. Block diagram of the proposed position-based discrete-time sliding mode impedance control (PBSMIC). The target impedance relationship is converted into the desired position trajectory x_d by resorting to the impedance filter. The position is controlled by DSMC directly and the force is regulated indirectly.

where $\mathrm{sgn}(\cdot)$ denotes the signum function and K_S is a positive control gain.

A block diagram of the proposed PBSMIC overall control scheme is shown in Fig. 2, where parameters d_p and s_p appear in (53) later.

B. Stability Analysis

Theorem 1: For the system (7) with the sliding function (18) and assumption (9), if the controller (25) is employed, then the discrete sliding mode will occur after a finite number of steps.

Proof: First, in view of (19), the sliding function (18) is expanded into the form

$$s_k = K_P e_k + K_I(e_k + \varepsilon_{k-1}) = G_a(x_k - x_{d,k}) + K_I\varepsilon_{k-1}. \quad (26)$$

Next, substituting (17) into (26) leads to

$$s_k = G_a\left\{\frac{1}{\bar{k}}\left[\bar{d}(u_k - u_{k-1}) + \bar{m}x_{k-3} + (\bar{b} - \bar{m})x_{k-2} + (\bar{k} - \bar{b})x_{k-1} - (F_k - F_{k-1}) - \tilde{p}_k\right] - x_{d,k}\right\} + K_I\varepsilon_{k-1}. \quad (27)$$

Then, obtaining the expression of the term $(u_k - u_{k-1})$ from (25) and substituting it into the sliding function (27), a necessary algebra operation gives

$$s_k = s_{k-1} - \frac{G_a K_S}{\bar{k}}\mathrm{sgn}(s_{k-1}) - \frac{G_a}{\bar{k}}\tilde{p}_k = s_{k-1} - \frac{G_a}{\bar{k}}\left[K_S\mathrm{sgn}(s_{k-1}) + \tilde{p}_k\right]. \quad (28)$$

Note that parameters $\bar{k}$, G_a, and K_S are all positive. In the case of $s_{k-1} \geq 0$, it can be derived that

$$s_k \leq s_{k-1} \quad \text{if} \quad K_S \geq |\tilde{p}_k|. \quad (29)$$

Otherwise, if $s_{k-1} < 0$, then

$$s_k \geq s_{k-1} \quad \text{if} \quad K_S \geq |\tilde{p}_k|. \quad (30)$$

Thus, in view of (29) and (30), the following conclusion can be drawn:

$$|s_k| \leq |s_{k-1}| \quad \text{if} \quad K_S \geq |\tilde{p}_k|. \quad (31)$$

In view of the assumption (9), the relationship (31) holds, which indicates that s_k decreases monotonously, and the discrete sliding mode is reached after a finite number of steps. ■

Remark 1: The relationship (31) represents a sufficient condition for the existence of discrete sliding mode [42]. Due to the discontinuity of the signum function $\mathrm{sgn}(\cdot)$, chattering may occur in the control input. To alleviate the chattering phenomenon, the boundary layer technique is adopted by replacing the signum function in (25) with the saturation function

$$\mathrm{sat}(s_k) = \begin{cases} \mathrm{sgn}(s_k), & \text{if } |s_k| > \delta \\ \frac{s_k}{\delta}, & \text{if } |s_k| \le \delta \end{cases} \tag{32}$$

where the parameter δ of the boundary layer thickness ensures that s_k is always bounded by $\pm\delta$. In practice, a tradeoff between the chattering and tracking error is needed to assign the parameter δ.

Remark 2: It is observed from (31) that the value of the discontinuous control gain K_S relies on the upper bound of the perturbation estimation error $|\tilde{p}_k|$. In the classical SMC, this term is the upper bound of the perturbation value [29]. Generally, the perturbation estimation error is much smaller than the actual perturbation, hence, a much smaller control gain can be achieved as compared with the corresponding classical SMC. In practice, the gain value K_S is tuned by the trial and error approach since no universal method is available yet [19].

IV. DSMIFC Scheme Design

In this section, an alternative DSMIFC scheme is proposed to directly ensure that the desired impedance behavior (12) is maintained by defining a sliding function based on the impedance measure error.

In view of the target impedance (12), the impedance measure error [23] can be defined as follows:

$$\epsilon_k = \bar{M}\tilde{e}_{k-2} + \bar{B}\tilde{e}_{k-1} + \bar{K}\tilde{e}_k + \bar{K}_f(F_k - F_{r,k}). \tag{33}$$

In the previous work [23], the impedance measure error is adopted as the sliding function to realize a sliding mode-based control. Alternatively, by taking into account the efficiency of integral action [18], a PI type of sliding function based on the impedance measure error is proposed in the current research to devise a new control scheme.

A. DSMIFC Design

Based upon the impedance measure error (33), a PI-type sliding function is proposed below

$$s_k = \tilde{K}_P\epsilon_k + \tilde{K}_I\zeta_k \tag{34}$$

where $\tilde{K}_P$ and $\tilde{K}_I$ are the positive proportional and integral gains, respectively. In addition, the integral impedance measure error is defined as

$$\zeta_k = \sum_{i=1}^{k}\epsilon_i = \epsilon_k + \zeta_{k-1}. \tag{35}$$

In view of (11), the impedance measure error (33) can be expanded into the form

$$\epsilon_k = \bar{M}\tilde{e}_{k-2} + \bar{B}\tilde{e}_{k-1} + \bar{K}(x_k - x_{r,k}) + \bar{K}_f(F_k - F_{r,k}). \tag{36}$$

Then, inserting the position x_k expressed by (17) into (36), results in

$$\begin{aligned}\epsilon_k = {} & \bar{M}\tilde{e}_{k-2} + \bar{B}\tilde{e}_{k-1} + \bar{K}\Big\{\frac{1}{\bar{k}}\big[d(u_k - u_{k-1}) + \bar{m}x_{k-3} \\ & + (\bar{b} - \bar{m})x_{k-2} + (\bar{k} - \bar{b})x_{k-1} - (F_k - F_{k-1}) - \tilde{p}_k\big]\Big\} \\ & - \bar{K}x_{r,k} + \bar{K}_f(F_k - F_{r,k}).\end{aligned} \tag{37}$$

Taking into account that the equivalent control u_k^{eq} is the solution to $\Delta s_k = s_k - s_{k-1} = 0$ [41], the following relationship can be deduced:

$$\tilde{K}_P\epsilon_k + \tilde{K}_I\zeta_k = s_{k-1} \tag{38}$$

$$\Rightarrow (\tilde{K}_P + \tilde{K}_I)\epsilon_k + K_I\zeta_{k-1} = s_{k-1}. \tag{39}$$

Substituting (37) into (39) and ignoring the estimation error $\tilde{p}_k$, gives the equivalent control action

$$\begin{aligned}u_k^{eq} = {} & u_{k-1} + \frac{\bar{k}}{\tilde{G}_a\bar{K}\bar{d}}(s_{k-1} - \tilde{K}_I\zeta_{k-1}) \\ & - \frac{\bar{k}}{\bar{K}\bar{d}}\big[\bar{M}\tilde{e}_{k-2} + \bar{B}\tilde{e}_{k-1} + \bar{K}_f(F_k - F_{r,k})\big] \\ & - \frac{1}{\bar{d}}\big[\bar{m}x_{k-3} + (\bar{b} - \bar{m})x_{k-2} + (\bar{k} - \bar{b})x_{k-1} \\ & - (F_k - F_{k-1})\big] + \frac{\bar{k}}{\bar{d}}x_{r,k}\end{aligned} \tag{40}$$

where $\tilde{G}_a = \tilde{K}_P + \tilde{K}_I$.

The equivalent controller (40) takes effect in the sliding phase when the impedance trajectory is kept on the sliding surface. However, if the initial impedance of the system does not lie on the sliding surface or severe uncertainties and disturbances (reflected by a large error $\tilde{p}_k$) occur during the sliding phase, the standalone equivalent control is not capable of driving the system impedance trajectory towards the sliding surface. In such scenarios, an additional control term u_k^{sw} is needed. Hence, the equivalent control is augmented by a discontinuous control to give the overall control action

$$u_k = u_k^{eq} + u_k^{sw}. \tag{41}$$

Specifically, the overall control is devised as

$$\begin{aligned}u_k = {} & u_{k-1} + \frac{\bar{k}}{\tilde{G}_a\bar{K}\bar{d}}(s_{k-1} - \tilde{K}_I\zeta_{k-1}) \\ & - \frac{\bar{k}}{\bar{K}\bar{d}}\big[\bar{M}\tilde{e}_{k-2} + \bar{B}\tilde{e}_{k-1} + \bar{K}_f(F_k - F_{r,k})\big] \\ & - \frac{1}{\bar{d}}\big[\bar{m}x_{k-3} + (\bar{b} - \bar{m})x_{k-2} + (\bar{k} - \bar{b})x_{k-1} \\ & - (F_k - F_{k-1})\big] + \frac{\bar{k}}{\bar{d}}x_{r,k} - \frac{\tilde{K}_S}{\bar{d}}\mathrm{sgn}(s_{k-1})\end{aligned} \tag{42}$$

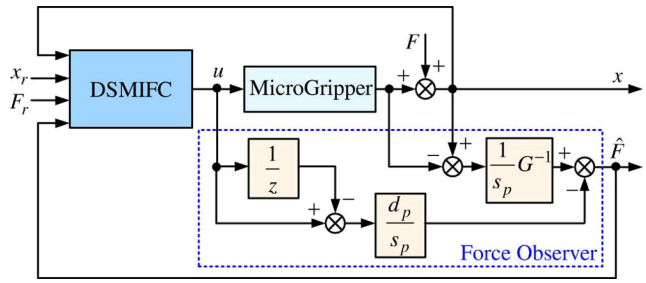

Fig. 3. Block diagram of the proposed discrete-time sliding mode impedance force control (DSMIFC). Both position error and force error is involved in the impedance measure error, which is suppressed by the DSMIFC algorithm. Both position and force are controlled directly.

where $\mathrm{sgn}(\cdot)$ denotes the signum function and $\tilde{K}_S$ is a positive control gain.

A block diagram representation of the proposed DSMIFC algorithm is depicted Fig. 3, where parameters d_p and s_p are presented in (53) later.

B. Stability Analysis

Theorem 2: For the system (7) with the sliding function (34) and assumption (9), if the controller (42) is adopted, then the discrete sliding mode will occur after a finite number of steps.

Proof: In view of (35), the sliding function (34) can be expanded as

$$\begin{aligned} s_k &= \tilde{K}_P\epsilon_k + \tilde{K}_I(\epsilon_k + \zeta_{k-1}) \\ &= \tilde{G}_a\epsilon_k + \tilde{K}_I\zeta_{k-1}. \end{aligned} \tag{43}$$

Then, inserting (37) into (43), gives

$$\begin{aligned} s_k = \tilde{G}_a &\left[\bar{M}\tilde{e}_{k-2} + \bar{B}\tilde{e}_{k-1} + \bar{K}_f(F_k - F_{r,k})\right] \\ &+ \frac{\tilde{G}_a\bar{K}}{\bar{k}}\left[\bar{d}(u_k - u_{k-1}) + \bar{m}x_{k-3} + (\bar{b} - \bar{m})x_{k-2}\right. \\ &\left. + (\bar{k} - \bar{b})x_{k-1}\right] - \tilde{G}_a\bar{K}x_{r,k} + K_I\zeta_{k-1}. \end{aligned} \tag{44}$$

Afterwards, generating the expression of $(u_k - u_{k-1})$ from (42) and substituting it into (44), the following equations are obtained after a necessary algebra operation:

$$\begin{aligned} s_k &= s_{k-1} - \frac{\bar{K}\tilde{K}_S}{\bar{k}}\mathrm{sgn}(s_{k-1}) - \frac{\bar{K}}{\bar{k}}\tilde{p}_k \\ &= s_{k-1} - \frac{\bar{K}}{\bar{k}}[\tilde{K}_S\mathrm{sgn}(s_{k-1}) + \tilde{p}_k] \end{aligned} \tag{45}$$

where parameters $\bar{k}$, $\bar{K}$, and $\tilde{K}_S$ are all positive.

In the case of $s_{k-1} \geq 0$, it can be derived that

$$s_k \leq s_{k-1} \quad \text{if} \quad \tilde{K}_S \geq |\tilde{p}_k|. \tag{46}$$

Otherwise, when $s_{k-1} < 0$, then

$$s_k \geq s_{k-1} \quad \text{if} \quad \tilde{K}_S \geq |\tilde{p}_k|. \tag{47}$$

Hence, in consideration of (46) and (47), as well as the assumption (9), the following deduction holds

$$|s_k| \leq |s_{k-1}| \quad \text{if} \quad \tilde{K}_S \geq |\tilde{p}_k| \tag{48}$$

which indicates that s_k decreases monotonously, and the discrete sliding mode is reached after a finite number of steps. ■

According to *Remark 1*, the relationship (48) represents a sufficient condition for the existence of discrete sliding mode [42]. In addition, to alleviate the chattering phenomenon, the boundary layer technique is adopted by replacing the signum function in (42) with a saturation function (32).

V. Theoretical Comparison and Analysis of the Two Control Schemes

A. Theoretical Comparison

Theoretically, both of the two new control schemes as developed in the foregoing sections are based on the GIC in conjunction with DSMC framework. However, they are implemented in different ways.

Specifically, the PBSMIC scheme is developed by transferring the target impedance relationship (10) into a desired position trajectory (16) by using the impedance filter (14). The DSMC algorithm (25) is then devised based on the PI-type sliding function (18) of the position tracking error. Hence, the position is controlled directly and the force is regulated indirectly in PBSMIC scheme. In contrast, the DSMIFC scheme is established on the basis of the impedance measure error (33), which incorporates both position and force tracking errors. Then, by defining a PI type of sliding function (34) of the impedance measure error, the DSMIFC strategy (42) is proposed. Thus, both position and force are directly regulated by the DSMIFC scheme.

The analyses of the steady-state errors of both schemes and their parameter selections are presented in the following discussions.

B. Steady-State Error Analysis and Impedance Parameters Selection

It has been shown that the dynamics of the environment affects the dynamics of the manipulator itself [43]. In this research, the contact environment that the microgripper encounters is modeled as follows [35]:

$$M_e\ddot{x} + B_e\dot{x} + K_e(x - x_e) = F \tag{49}$$

where M_e, B_e, and K_e describe the mass, damping, and stiffness of the environment, respectively. In addition, x_e represents the equilibrium position of the environment in the absence of interaction force.

Then, combing (10) and (49) allows the generation of an equation of the closed-loop impedance control system interacting with the environment

$$\begin{aligned} &(M + K_fM_e)\ddot{x} + (B + K_fB_e)\dot{x} + (K + K_fK_e)x \\ &\qquad = M\ddot{x}_r + B\dot{x}_r + Kx_r + K_f(F_r + K_ex_e) \end{aligned} \tag{50}$$

which is stable if the desired impedance parameters are chosen as positive values.

To enable the microgripper a satisfactory manipulation with desired interaction behavior, the relationship between the desired position (x_r) and force (F_r) trajectories and the target impedance parameters (M, B, K, and K_f) should be

well planned in consideration of the environment property. According to the assembly/manipulation strategy as presented in [29] and [35], a compromise between position and force control can be achieved by adjusting the two sets of impedance parameters $\{M, B, K\}$ and $\{K_f\}$, which are related to the position and force, respectively.

At the steady state, the position and force errors can be calculated from response of the closed-loop system (50) as follows:

$$E_x = \frac{F_r + K_e(x_e - x_r)}{K_e + \frac{K}{K_f}} \tag{51}$$

$$E_f = -\frac{K}{K_f} E_x. \tag{52}$$

It can be observed that if K_e is relatively small and $K \gg K_f$ is assigned, then the steady-state position error E_x is relatively small, whereas the steady-state force error E_f is relatively large. Hence, the position control is emphasized. On the contrary, if K_e is relatively large and $K \ll K_f$ is chosen, then the force control is emphasized and the desired force is tracked more accurately than the position. Consequently, a balance between the position and force tracking control can be implemented by adjusting the relative values of target impedance parameters K and K_f. In addition, the impedance parameters M and B can be selected to achieve a desired transient response of the closed-loop system (50).

In the preceding discussions, the environment model (49) is only employed for the steady-state error analysis of the position and force control. The transient response of the interaction behavior is governed by the defined generalized impedance (10). Concerning the influence of environment on the control aspects, impedance control possesses some inherent robustness to environment uncertainty [28]. Hence, the role of environment is not explicitly considered here. In the subsequent section, the theoretical analyses are validated by experimental studies.

VI. Experimental Studies

The developed position/force interaction control schemes are verified by conducting several experimental studies on a prototype microassembly system in this section.

A. Experimental Setup

The experimental setup of a piezoelectric microgripper system is depicted in Fig. 4. The microgripper is composed of two piezoelectric multimorph actuators (consisting of four piezolayers and one inner brass layer) with the dimension of $26 \times 5 \times 0.86\ \mathrm{mm}^3$, i.e., the thickness of each multimorph is 860 μm (see close-up view in Fig. 4). In this research, one of two piezoelectric actuators is driven by a high-voltage amplifiers (model: EPA-104 from Piezo Systems, Inc.). The end-point position of the gripper arm is measured by a laser displacement sensor (model: LK-H055, from Keyence Corporation). The laser sensor provides a resolution of 25 nm within a measuring range of 20 mm around the reference distance of 50 mm, which enables a large free space for microassembly tasks. A digital microscope ($\mathrm{magnification\ ratio} = 200$) is mounted above the microgripper to monitor the assembly process. In addition, a NI cRIO-9075 real-time controller (from National Instruments Corporation) equipped with NI-9263 analogy output module and NI-9870 RS-232 serial interface module is adopted to produce analogy excitation signals and acquire digital sensor readings. Moreover, LabVIEW software is employed to implement a deterministic real-time control of the system.

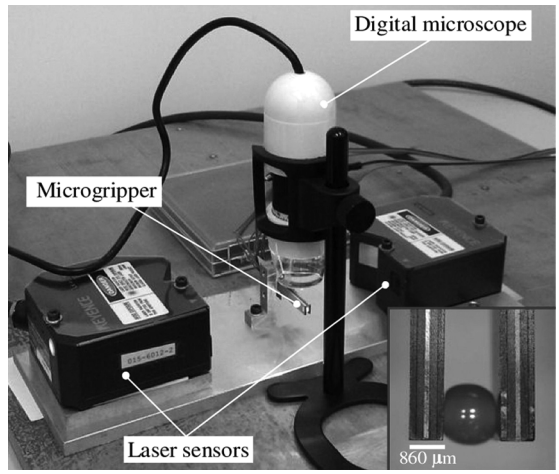

Fig. 4. Experimental setup of a piezoelectric microgripper system for gripping a glass microbead. The microgripper is composed of two four-layer piezoelectric multimorphs with brass reinforced inner layers.

The micro-object to be grasped is a glass microbead ($\mathrm{diameter} = 1400\ \mu\mathrm{m}$) as shown in the close-up view in Fig. 4. To demonstrate the capability of the presented control schemes for simultaneous position and force control, only the left gripper arm is employed in the experiments, whereas the right one acts as a passive arm.

B. Force Estimator Development

In this paper, a force estimator as proposed in recent work [44] of the author is employed to reconstruct the force signal. The uniqueness of the method lies in that neither hysteresis model nor creep model is required. The force estimator is briefly described below. More details about its implementation can be found in [44].

The force that is experienced by the microgripper arm is estimated in the time domain

$$\hat{F}(t) = \frac{1}{s_p}\mathscr{T}^{-1}\{G^{-1}(s)\}[x(t) - x_1(t)] - \frac{d_p}{s_p}[u(t) - u(t-T)] \tag{53}$$

where $u(t)$ and $u(t-T)$ denote the excitation voltages applied to the high-voltage amplifier at the time instance t and $t-T$, respectively. The position output x is contributed by both excitation voltage u and applied force F, whereas the position output x_1 is excited by the voltage u alone. Additionally, $\mathscr{T}^{-1}$ represents the inverse Laplace transform operator, and $G(s)$ (with unity DC gain) is the plant model under the excitation of input voltage. Besides, d_p and s_p are the piezoelectric constant and elastic constant of the piezoelectric multimorph, respectively.

When the excitation voltage u is applied alone (i.e., $F = 0$), the plant model is identified by the swept-sine method. The magnitude of the frequency response is shown in Fig. 5. It is observed that the identified second-order model G_p matches

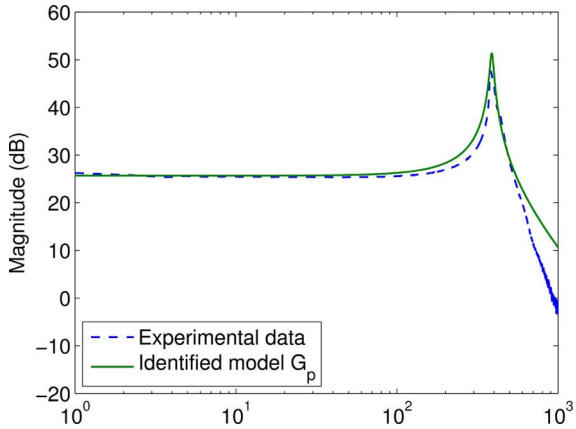

Fig. 5. Magnitude plot of the frequency response of the system. The identified second-order model G_p captures the system dynamics up to 500 Hz.

the system dynamics well in low frequencies up to 500 Hz. To capture the high-frequency behavior, a much higher order model is required to be identified. In this research, the simple second-order model is employed to demonstrate the effectiveness of the proposed control schemes.

The piezoelectric constant d_p is calculated as the DC gain value of G_p, i.e., $d_p = 19.0\ \mu\text{m/V}$. Then, the plant model G with unity DC gain is computed by $G = G_p/d_p$, i.e.,

$$G(s) = \frac{5.9430 \times 10^6}{s^2 + 126.8\, s + 5.9430 \times 10^6}. \tag{54}$$

In addition, the elastic constant s_p of the cantilever is determined below by hanging a known weight and recording the induced displacement at steady state

$$s_p = \frac{11.5\ \mu\text{m}}{25\ \text{mN}} = 0.46\ \frac{\mu\text{m}}{\text{mN}}. \tag{55}$$

By using the force signal provided by the force estimator (53), experiments on interaction control of the microgripper dedicated to microassembly are conducted by gripping a microbead in the following discussions.

First of all, a voltage signal as shown in Fig. 6(a) is applied to drive the gripper arm in order to examine the performance of the force estimator. Without the external force applied, the position response is shown in Fig. 6(b), and the force estimator output is depicted in Fig. 6(d). It is found that the force is accurately estimated with a root-mean-square error (RMSE) of 0.26 mN. Besides, an open-loop hysteresis loop of the piezoelectric gripper arm is illustrated in Fig. 6(c), which poses a challenge to the impedance control.

C. Controller Setup

1) Concurrent Trajectory Planning: In this research, the microbead to be gripped is in contact with the gripper arms initially. To conduct an impedance control, a position trajectory x_r and a corresponding force trajectory F_r need to be planned concurrently.

By applying the excitation voltage as shown in Fig. 7(a) to the gripper arm (with interaction force applied), the induced position and force signals are shown in Fig. 7(b) and (c) (solid lines). Note that the negative sign of the signal indicates that the force is exerted on the gripper arm. The relationship between the

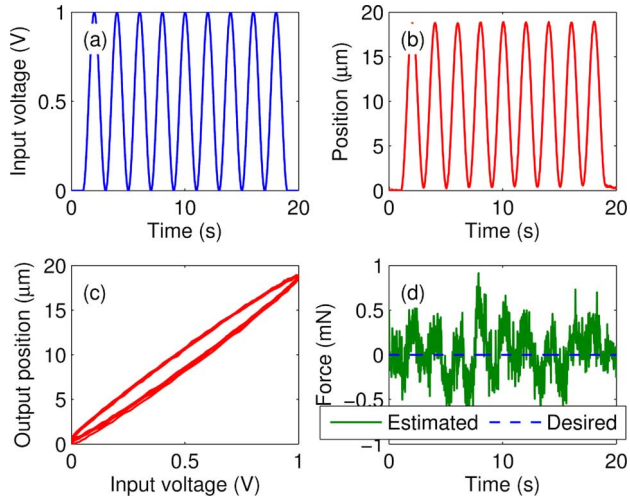

Fig. 6. (a) Input voltage signal. (b) Output position. (c) Position-voltage hysteresis loop. (d) Force estimation result of the force observer without applied force.

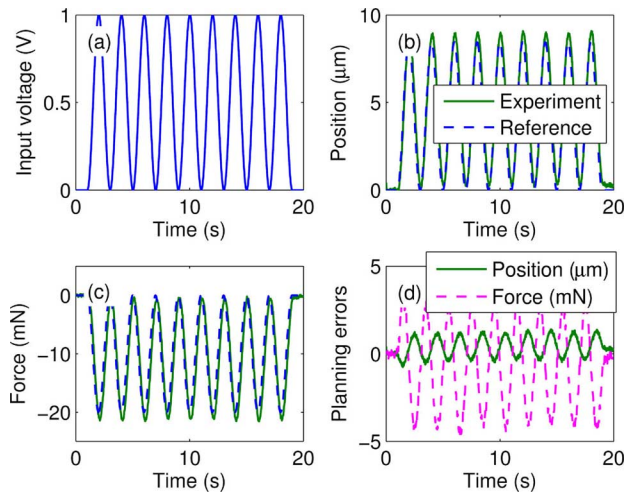

Fig. 7. (a)–(c) Force estimation result of the force observer with force applied. (d) Trajectory planning errors between the planned position and force trajectories and actual ones, respectively.

peak-to-peak (pp) magnitudes of the position and force signals excited by four voltage levels (with pp values of 0.3, 1, 1.5, and 2 V) is depicted in Fig. 8. A least-square linear fit of the four points determines a linear relationship. This line relates the displacement penetrated into the environment to the magnitude of the interaction force, and it provides a guideline for the concurrent planning of the position and force trajectories.

For illustration, the pp magnitude of the reference position trajectory is specified as $8.45\ \mu\text{m}$. Thus, the concurrent force trajectory is planned with a pp magnitude of $-20.0\ \text{mN}$ according to Fig. 8. The planned trajectories are shown in Fig. 7(b) and (c) (dashed lines). Fig. 7(d) depicts the errors between the planned position and force trajectories and the actual ones.

It is noticed that the linear relationship in Fig. 8 implies a stiffness value of $2.47\ \text{mN}/\mu\text{m}$, which is slightly higher than the value of $2.17\ \text{mN}/\mu\text{m}$ as calculated by (55). The reason arises from the fact that the latter represents the steady-state (static) value, whereas the former denotes a dynamic value with an input frequency of 0.5 Hz. Due to the hysteresis effect of

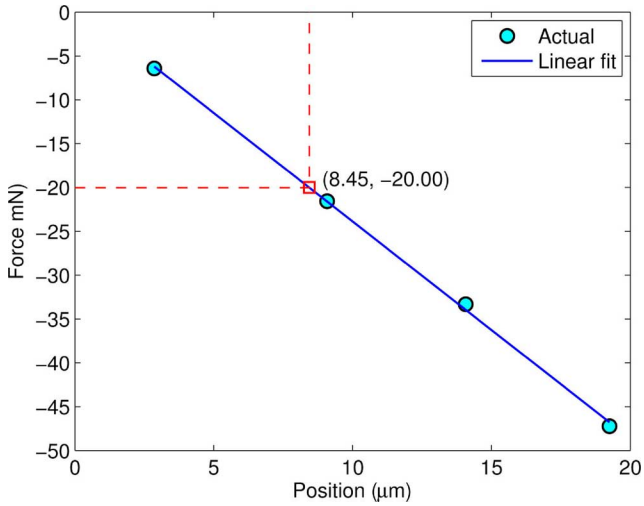

Fig. 8. Relationship between the pp magnitudes of the planned position and force trajectories.

the piezoelectric actuator, the higher the input rate, the smaller the motion range (i.e., the pp magnitude of position). Thus, the stiffness value calculated from a dynamic signal is higher than the static one.

2) Dynamics and Impedance Parameters Setting: Concerning the dynamics model parameters, the mass of one piezoelectric multimorph is chosen as its nominal value of $m = 1.8 \times 10^{-3}$ kg for the reason of simplicity. Actually, the effective mass is lower than the nominal value. More detailed analysis is required to determine the actual effective mass value in the future. In addition, by comparing model (1) with the inverse Laplace transform of plant model G_p, other parameters are obtained as: $b = 126.8\ \mathrm{N\,s}/\mu\mathrm{m}$, $k = 5.943 \times 10^6\ \mathrm{N}/\mu\mathrm{m}$, and $d = 1.129 \times 10^8\ \mu\mathrm{m/V}$.

Since the right gripper arm is passive, this arm and the microbead to be grasped together act as the environment in this research. In view of the compliance of the piezo-cantilever as given in (55), the stiffness is calculated as $2.17 \times 10^3\ \mathrm{N/m}$. Considering that the rigidity of glass microbead is much higher than that of the gripper arm, the environment stiffness of $K_e \approx 2 \times 10^3\ \mathrm{N/m}$ is assumed. Other desired parameters in the target impedance (10) are selected as: $M = 1$, $B = 2\zeta\omega_n$, and $K = \omega_n^2$, where $\zeta = 1$ is set to achieve a critical damping.

Concerning the position-based impedance control, it has been shown in [45] that the target stiffness K should be higher than twice the environment stiffness in order to avoid the oscillatory behavior. In the current research, $\omega_n = 1420\pi\ \mathrm{rad/s}$ is chosen to give the target parameters: $B = 8.9221 \times 10^3\ \mathrm{N\,s/m}$ and $K = 1.9901 \times 10^7\ \mathrm{N/m}$.

In view of the relationship (52), K_f should be chosen to constrict the maximum force to guarantee that the gripper and manipulated micro-object are not damaged. With the planned reference position and force trajectories, it is observed from Fig. 7(d) that the maximum position error of 1 μm occurs when the force error is -4 mN. Thus, K_f is selected as $K_f = K/4 \approx 5000\ (\mathrm{mN/mN})$. Hence, $K > K_f$ holds, which indicates that the position control is emphasized in the impedance control.

With a sampling time $T = 0.02$ s, the discrete-time model and impedance parameters are calculated by (5) and (13), respectively, and the experiments are conducted below.

D. Position and Force Tracking Control Results

1) PBSMIC Results: Concerning the PBSMIC controller, the control gains are tuned by several trials as: $K_P = 5$, $K_I = 1$, $K_S = 0.003$, and $\delta = 100$. The tracking results are depicted in Fig. 9. It is observed from Fig. 9(a)–(d) that both the position and force trajectories are well tracked with the maximum errors of 0.89 μm and 3.44 mN, respectively. The control input as shown in Fig. 9(e) reveals that no chattering phenomenon exists. In addition, Fig. 9(f) indicates that the sliding function is well constrained by the boundary layer parameter $\delta = 100$.

As the control gain K_P decreases from 5 to 0.5, more experiments are carried out. The position and force tracking results of PBSMIC are summarized in Table I, where the position and force relative RMSEs are calculated as the percent RMSEs with respect to the pp magnitudes of position and force trajectories, respectively.

2) DSMIFC Results: Regarding the DSMIFC controller, the gain parameters are tuned as: $\tilde{K}_P = 2$, $\tilde{K}_I = 1$, $\tilde{K}_S = 10^3$, and $\tilde{\delta} = 10^6$. The tracking results as shown in Fig. 10 exhibit that the maximum position and force tracking errors are 1.39 μm and 3.45 mN, respectively. In addition, Fig. 10(e) displays that no chattering exists in the control action, and the role of the boundary layer $\tilde{\delta} = 10^6$ is evident from the sliding function as depicted in Fig. 10(f). It is noticeable that the tracking accuracy can be improved by tuning the control gains more appropriately.

To illustrate the effect of relative value selection of the impedance parameters K and K_f on the tracking performance, the DSMIFC with K_f varying from 0 to 6000 is tested. For each K_f value, five sets of experimental data are obtained. The error bars of relative RMSEs for both position and force tracking results versus K_f are plotted in Fig. 11.

E. Discussions

Concerning the PBSMIC results as shown in Table I, it is seen that the smaller the control gain K_P, the smaller the position tracking error. As a position-based controller, the result seems to violate the general sense that the higher the control gain, the smaller the tracking error. The reason can be explained by inspecting the control input (25), which reveals that the concerned items of control action are in inverse proportional to the control gain G_a (i.e., $K_P + K_I$). Thus, a smaller control gain produces a larger control action, which leads to a smaller position error. However, further decrease of K_P causes instability of the control system. Additionally, it is found that as the control gain varies, the position error and force error change in opposite tendencies. That is, a good position tracking is achieved at the sacrifice of force accuracy, and *vice versa*. The results imply that the position tracking accuracy and force tracking accuracy can be compromised by adjusting the control gains for the PBSMIC scheme. In addition, the fact that the position and force errors can be suppressed to a low level indicates the robustness of the control scheme regarding the open-loop hysteresis loop as shown in Fig. 6(c).

As far as DSMIFC scheme is concerned, it is observed from Fig. 11 that as K_f increases from 0 to 5000, the position error is increased gradually as predicted by (51). Whereas the force error reduces as the rising of K_f, which agrees well with the prediction of (52). Moreover, it is found that the magnitude of

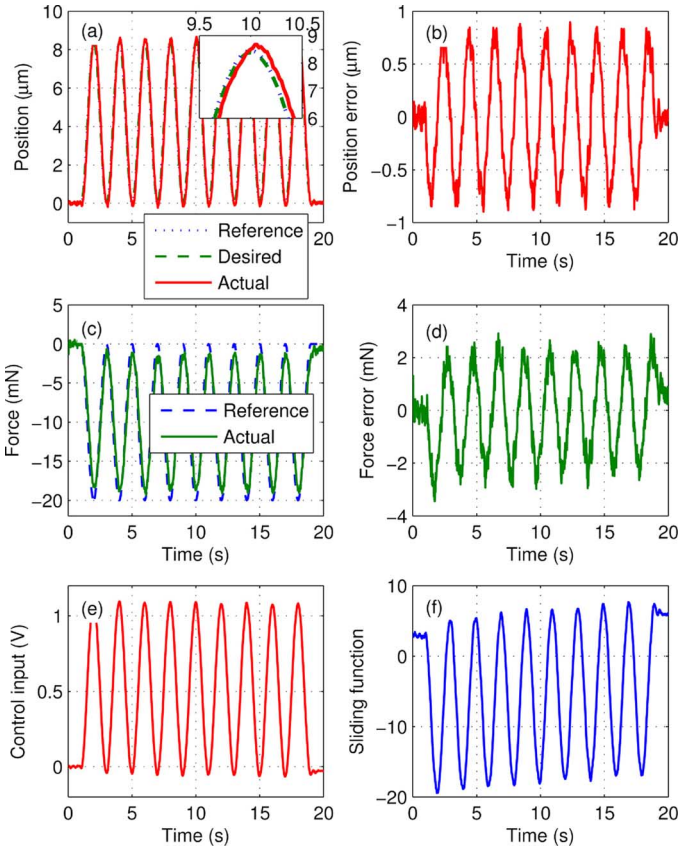

Fig. 9. Tracking control results of PBSMIC with the control gain $K_P = 1$.

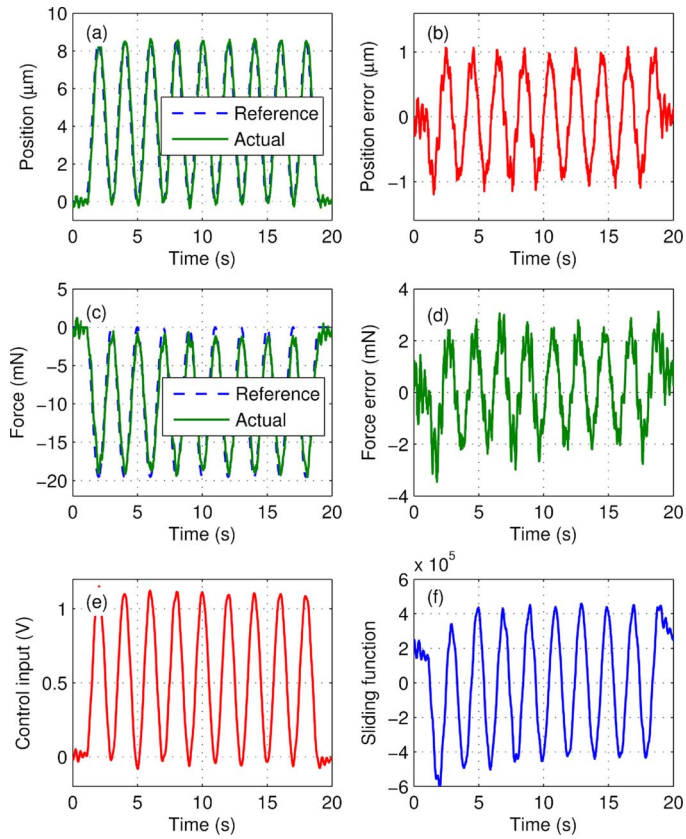

Fig. 10. Tracking control results of DSMIFC with the target impedance parameter $K_f = 5 \times 10^3$.

TABLE I
POSITION AND FORCE TRACKING RESULTS OF PBSMIC WITH DIFFERENT CONTROL GAINS K_P

PBSMIC controller	Position RMSE (μm)	Relative RMSE (%)	Force RMSE (mN)	Relative RMSE (%)
K_P = 5	1.3710	16.22	0.5620	2.81
K_P = 2	0.7519	8.90	1.1557	5.78
K_P = 1	0.5119	6.06	1.5532	7.77
K_P = 0.5	0.4069	4.82	1.8454	9.23

the position relative RMSE is smaller than that of the force relative RMSE. The reason lies in the fact that the relationship of $K > K_f$ holds, i.e., the position control is emphasized in the impedance control as assessed in Section V. As a result, a relative small position tracking error is achieved. Fig. 11 also illustrates how to select a balance point of the position and force tracking. It is observed that in the case of $K_f = 4000$, a better balance between the position and force tracking accuracy is achieved since DSMIFC produces both errors around 8.1%. As K_f further increases from 4000, the force control is more emphasized. However, it is found that a too large K_f has the same effect as a large control gain, which induces oscillation in the control action. For instance, $K_f = 6000$ produces moderate oscillation in the tracking control which deteriorates both position and force tracking accuracy as described in Fig. 11.

Further experiments demonstrate that the balance of position and force tracking can be achieved for both control schemes by adjusting either control gains (e.g., K_P) or target impedance parameters (e.g., K_f). Moreover, the tracking errors

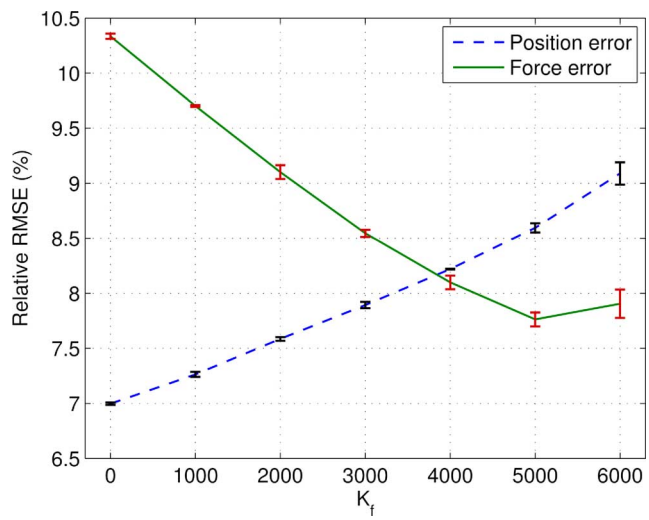

Fig. 11. Position and force tracking relative RMSEs of DSMIFC versus the target impedance parameter K_f.

of DSMIFC as shown in Fig. 11 can be reduced by adjusting the control gains. As compared with impedance parameters, the control gains influence the tracking results more significantly. Regarding the selection of parameter ω_n which determines the impedance parameters B and K, additional experimental tests reveal that the larger the ω_n value, the smaller the achievable position and force tracking errors for the two schemes. The conducted experimental studies reveal that the interaction between the microgripper and microbead is precisely regulated.

As a result, the slip of the microbead is prevented and the safety of both the gripper and the gripped object is guaranteed. It is noted that the gains of K_S and $\tilde{K}_S$ are tuned by trial and error methods in the experiments.

Owing to the limitation of the employed hardware, a sampling time of $T = 0.02$ s is implemented in the preceding experimental studies. As compared with the resonant frequency of 388 Hz of the system (see Fig. 5), the sampling frequency of 50 Hz is relatively low (which is typical for a visual servoing system [3]). With such a sampling rate, the conventional continuous-time sliding mode control may not work well if directly deployed to the sampled-data system. Hence, the effectiveness of the proposed discrete-time control schemes is evident from the experimental results.

Due to the low bandwidth as a consequence of low sampling rate, sinusoidal trajectories for both position and contact force are carried out. Actually, other trajectories (e.g., step and triangle) can also be employed for the illustration of the effectiveness of the proposed control schemes. However, such trajectories contain high-frequency harmonics, which inevitably excite high-frequency dynamics out of range of the control bandwidth. In the next step, higher sampling frequency will be implemented to examine the performance of the proposed control schemes for high-frequency trajectory tracking. In addition, the force signal is provided by a force observer. The estimation error may occur in practice. It is assumed that the force estimation error is negligible in this research. The investigation on how to deal with this force error is under way.

As an impedance control, the proposed control schemes are capable of regulating the position and contact force simultaneously. Nevertheless, the reference position and force trajectories cannot be assigned independently. For instance, once the position trajectory is assigned, the reference force trajectory should be defined according to the stiffness of the environment and of the actuator. The concurrent trajectory planning is illustrated in Fig. 8. It is also noticeable that the gain values of the PBSMIC and DSMIFC controllers are not optimally designed in the preceding experiments. The current amplitudes of the position and force tracking RMSEs indicate that the performances of the control schemes may be improved to further enhance the tracking accuracy. In the future, the issue of extending the proposed control schemes to higher order systems and multiple-input and multiple-output (MIMO) systems will be investigated as well.

VII. Conclusion

This paper proposes two new control schemes for simultaneous position/force tracking control of a piezoelectric multimorph microgripper dedicated to microassembly application. Different from classical control method which implements the position control of one gripper arm and force control of the other one, the proposed approaches are capable of regulating both position and force simultaneously for each arm. This feature enables a more reliable and safer manipulation and allows the actuation of one single gripper arm for both position and force control, which reduces the hardware cost of the microgripper system. Results have shown that both schemes are capable of achieving satisfactory position and force tracking results, and a balance between the position and force accuracy can be easily achieved by adjusting the relative values of control gains or target impedance parameters. The reported methodology can be extended for the interaction control of other types of microgrippers as well.

References

[1] D. J. Cappelleri, P. Cheng, J. Fink, B. Gavrea, and V. Kumar, "Automated assembly for mesoscale parts," *IEEE Trans. Automat. Sci. Eng.*, vol. 8, no. 3, pp. 598–613, Jul. 2011.

[2] V. Eichhorn, M. Bartenwerfer, and S. Fatikow, "Nanorobotic assembly and focused ion beam processing of nanotube-enhanced AFM probes," *IEEE Trans. Automat. Sci. Eng.*, vol. 9, no. 4, pp. 679–686, Oct. 2012.

[3] J. D. Wason, J. T. Wen, J. J. Gorman, and N. G. Dagalakis, "Automated multiprobe microassembly using vision feedback," *IEEE Trans. Robot.*, vol. 28, no. 5, pp. 1090–1103, Oct. 2012.

[4] F. Beyeler, A. Neild, S. Oberti, D. J. Bell, Y. Sun, J. Dual, and B. J. Nelson, "Monolithically fabricated microgripper with integrated force sensor for manipulating microobjects and biological cells aligned in an ultrasonic field," *J. Microelectromech. Syst.*, vol. 16, no. 1, pp. 7–15, Feb. 2007.

[5] K. Kim, X. Liu, Y. Zhang, and Y. Sun, "Nanonewton force-controlled manipulation of biological cells using a monolithic MEMS microgripper with two-axis force feedback," *J. Micromech. Microeng.*, vol. 18, no. 5, p. 055013, May 2008.

[6] M. Grossard, C. Rotinat-Libersa, N. Chaillet, and M. Boukallel, "Mechanical and control-oriented design of a monolithic piezoelectric microgripper using a new topological optimization method," *IEEE/ASME Trans. Mechatron.*, vol. 14, no. 1, pp. 32–45, Feb. 2009.

[7] M. Rakotondrabe, C. Clévy, and P. Lutz, "Complete open loop control of hysteretic, creeped and oscillating piezoelectric cantilevers," *IEEE Trans. Automat. Sci. Eng.*, vol. 7, no. 3, pp. 440–450, Jul. 2010.

[8] C. V. Newcomb and I. Flinn, "Improving the linearity of piezoelectric ceramic actuators," *Electron. Lett.*, vol. 18, no. 11, pp. 442–444, Nov. 1982.

[9] G. M. Clayton, S. Tien, A. J. Fleming, S. O. R. Moheimani, and S. Devasia, "Inverse-feedforward of charge-controlled piezopositioners," *Mechatronics*, vol. 18, no. 5-6, pp. 273–281, Jun. 2008.

[10] B. J. G. Vautier and S. O. R. Moheimani, "Charge driven piezoelectric actuators for structural vibration control: Issues and implementation," *Smart Mater. Struct.*, vol. 14, no. 4, pp. 575–586, Aug. 2005.

[11] M. Al Janaideh, S. Rakheja, and C. Su, "An analytical generalized Prandtl-Ishlinskii model inversion for hysteresis compensation in micropositioning control," *IEEE/ASME Trans. Mechatron.*, vol. 16, no. 4, pp. 734–744, Aug. 2011.

[12] Q. Xu, "Identification and compensation of piezoelectric hysteresis without modeling hysteresis inverse," *IEEE Trans. Ind. Electron.*, 2012, in press, DOI: 10.1109/TIE.2012.2206339.

[13] F. Krohs, C. Onal, M. Sitti, and S. Fatikow, "Towards automated nanoassembly with the atomic force microscope: A versatile drift compensation procedure," *J. Dyn. Sys., Meas., Control*, vol. 131, no. 6, p. 061106, 2009.

[14] A. S. Putra, S. Huang, K. K. Tan, S. K. Panda, and T. H. Lee, "Design, modeling, and control of piezoelectric actuators for intracytoplasmic sperm injection," *IEEE Trans. Contr. Syst. Technol.*, vol. 15, no. 5, pp. 879–890, Sep. 2007.

[15] Q. Xu, "Design and development of a flexure-based dual-stage nanopositioning system with minimum interference behavior," *IEEE Trans. Automat. Sci. Eng.*, vol. 9, no. 3, pp. 554–563, Jul. 2012.

[16] Q. Xu and Y. Li, "Micro-/nanopositioning using model predictive output integral discrete sliding mode control," *IEEE Trans. Ind. Electron.*, vol. 59, no. 2, pp. 1161–1170, Feb. 2012.

[17] X. Yu and O. Kaynak, "Sliding-mode control with soft computing: A survey," *IEEE Trans. Ind. Electron.*, vol. 56, no. 9, pp. 3275–3285, Sep. 2009.

[18] J.-X. Xu and K. Abidi, "Discrete-time output integral sliding-mode control for a piezomotor-driven linear motion stage," *IEEE Trans. Ind. Electron.*, vol. 55, no. 11, pp. 3917–3926, Nov. 2008.

[19] Y. Li and Q. Xu, "Adaptive sliding mode control with perturbation estimation and PID sliding surface for motion tracking of a piezo-driven micromanipulator," *IEEE Trans. Contr. Syst. Technol.*, vol. 18, no. 4, pp. 798–810, Jul. 2010.

[20] K. Rabenorosoa, C. Clévy, and P. Lutz, "Active force control for robotic micro-assembly: Application to guiding tasks," in *Proc. IEEE Int. Conf. Robot. Autom.*, Anchorage, AK, USA, 2010, pp. 2137–2142.

[21] M. Rakotondrabe and I. A. Ivan, "Development and force/position control of a new hybrid thermo-piezoelectric microgripper dedicated to micromanipulation tasks," *IEEE Trans. Automat. Sci. Eng.*, vol. 8, no. 4, pp. 824–834, Oct. 2011.
[22] M. C. Carrozza, A. Eisinberg, A. Menciassi, D. Campolo, S. Micera, and P. Dario, "Towards a force-controlled microgripper for assembling biomedical microdevices," *J. Micromech. Microeng.*, vol. 10, no. 2, p. 271, Jun. 2000.
[23] Z. Lu, S. Kawamura, and A. A. Goldenberg, "An approach to sliding-mode based control," *IEEE Trans. Robot. Automat.*, vol. 11, no. 5, pp. 754–759, 1995.
[24] H. Seraji and R. Colbaugh, "Force tracking in impedance control," *Int. J. Robot. Research*, vol. 16, no. 1, pp. 97–117, Feb. 1997.
[25] W.-S. Lu and Q.-H. Meng, "Impedance control with adaptation for robotic manipulations," *IEEE Trans. Robot. Automat.*, vol. 7, no. 3, pp. 408–415, Jun. 1991.
[26] S. Lee and H. Lee, "Intelligent control of manipulators interacting with an uncertain environment based on generalized impedance," in *Proc. IEEE Int. Symp. Intell. Control*, Arlington, VA, USA, 1991, pp. 61–66.
[27] S. Jung, T. C. Hsia, and R. G. Bonitz, "Force tracking impedance control for robot manipulators with an unknown environment: Theory, simulation, and experiment," *Int. J. Robot. Research*, vol. 20, no. 9, pp. 765–774, Sep. 2001.
[28] F. Almeida, A. Lopes, and P. Abreu, "Force-impedance control: A new control strategy of robotic manipulators," in *Recent Advances in Mechatronics*, O. Kaynak, S. Tosunoglu, and M. H. J. Ang, Eds. New York, NY, USA: Springer, 1999, pp. 126–137.
[29] H. C. Liaw and B. Shirinzadeh, "Robust generalised impedance control of piezo-actuated flexure-based four-bar mechanisms for micro/nano manipulation," *Sens. Actuator A-Phys.*, vol. 148, no. 2, pp. 443–453, Dec. 2008.
[30] J. J. Gorman and N. G. Dagalakis, "Force control of linear motor stages for microassembly," in *Proc. ASME Int. Mech. Eng. Congr. Exposit.*, Washington, DC, USA, 2003, pp. 615–623.
[31] Y. Xie, D. Sun, H. Y. G. Tse, C. Liu, and S. H. Cheng, "Force sensing and manipulation strategy in robot-assisted microinjection on zebrafish embryos," *IEEE/ASME Trans. Mechatron.*, vol. 16, no. 6, pp. 1002–1010, Dec. 2011.
[32] A. Ibeas and M. de la Sen, "Robust sliding control of robotic manipulators based on a heuristic modification of the sliding gain," *J. Intell. Robot. Syst.*, vol. 48, no. 4, pp. 485–511, Mar. 2007.
[33] S. Chen, W. Harwin, and T. Rahman, "The application of discrete-time adaptive impedance control to rehabilitation robot manipulators," in *Proc. IEEE Int. Conf. Robot. and Autom.*, San Diego, CA, USA, 1994, pp. 636–642.
[34] C. H. Houpis and G. B. Lamont, *Digital Control Systems: Theory, Hardware, Software*, 2nd ed. New York, NY, USA: McGraw-Hill, 1992.
[35] S. P. Chan and H. C. Liaw, "Generalized impedance control of robot for assembly tasks requiring compliant manipulation," *IEEE Trans. Ind. Electron.*, vol. 43, no. 4, pp. 453–461, Aug. 1996.
[36] T. S. Low and W. Guo, "Modeling of a three-layer piezoelectric bimorph beam with hysteresis," *J. Microelectromech. Syst.*, vol. 4, no. 4, pp. 230–237, Dec. 1995.
[37] Q. Xu and Y. Li, "Model predictive discrete-time sliding mode control of a nanopositioning piezostage without modeling hysteresis," *IEEE Trans. Contr. Syst. Technol.*, vol. 20, no. 4, pp. 983–994, Jul. 2012.
[38] M. Tarokh, "A discrete-time adaptive control scheme for robot manipulators," *J. Robotic Syst.*, vol. 7, no. 2, pp. 145–166, Apr. 1990.
[39] H. Elmali and N. Olgac, "Implementation of sliding mode control with perturbation estimation (SMCPE)," *IEEE Trans. Control Syst. Technol.*, vol. 4, no. 1, pp. 79–85, 1996.
[40] N. Hogan, "Impedance control: An approach to manipulation: Parts I–III," *J. Dyn. Sys., Meas., Control*, vol. 107, no. 1, pp. 1–24, 1985.
[41] K. Furuta, "Sliding mode control of a discrete system," *Syst. Control Lett.*, vol. 14, no. 2, pp. 145–152, Feb. 1990.
[42] S. Sarpturk, Y. Istefanopulos, and O. Kaynak, "On the stability of discrete-time sliding mode control systems," *IEEE Trans. Automat. Contr.*, vol. 32, no. 10, pp. 930–932, Oct. 1987.
[43] S. Eppinger and W. Seering, "On dynamic models of robot force control," in *Proc. IEEE Int. Conf. Robot. Autom.*, San Francisco, CA, USA, 1986, vol. 3, pp. 29–34.
[44] Q. Xu, "A new method of force estimation in piezoelectric cantilever-based microgripper," in *Proc. IEEE/ASME Int. Conf. Adv. Intell. Mechatronics*, KaoHsiung, Taiwan, 2012, pp. 574–579.
[45] B. Heinrichs and N. Sepehri, "A limitation of position based impedance control in static force regulation: Theory and experiments," in *Proc. IEEE Int. Conf. Robot. Autom.*, Detroit, MI, USA, 1999, pp. 2165–2170.

Qingsong Xu (M'09) received the B.S. degree in mechatronics engineering (Hons.) from the Beijing Institute of Technology, Beijing, China, in 2002, and the M.S. and Ph.D. degrees in electromechanical engineering from the University of Macau, Macao, China, in 2004 and 2008, respectively.

He was a Visiting Scholar at the Swiss Federal Institute of Technology (ETH), Zurich, Switzerland, and the National University of Singapore (NUS), Singapore. He is currently an Assistant Professor of Electromechanical Engineering with the University of Macau. His current research interests include MEMS devices, micro/nanosystems, micro/nanoassembly, smart materials and structures, and computational intelligence.

Dr. Xu is a member of the American Society of Mechanical Engineers (ASME). He currently serves on the editorial boards or as guest editors of six international journals.